Supplemental Material

Novel RANK antagonists for the treatment of bone resorptive disease: Theoretical predictions and experimental validation

Stéphane Téletchéa[1†‡], Verena Stresing[1†‡], Soizic Hervouet[1‡], Marie-Françoise Heymann[1‡], Gildas Bertho[2], Céline Charrier[1‡], Kosei Ando[1‡], Dominique Heymann[1‡*]

SUPPLEMENTAL MATERIALS AND METHODS

Generation of a library of soluble random peptides

To identify new inhibitors of the RANK/RANKL interaction, peptide sequences of variable length (approximately 100 million sequences) were generated in silico through a perl iterator on a dual quad-core 2.66 Ghz Xeon 5630 workstation. Amino acids (AA) were selected randomly using the perl rand() function from the 20 naturally occurring amino acids. The length of the sequences was arbitrarily limited to 7 to 13 AAs. The perl random generator provided sufficiently different sequences which were then submitted to the validation procedure.

Peptide sequences were filtered based on their 1D sequence to ensure their solubility in biologically compatible solvents for experimental validation, using the following criteria: Sequences starting or ending with a charged amino acid were discarded, since this may increase the cost of synthesis and/or purification. A sequence was discarded if it contained more than one glycine (G) or proline (P), since these residues are known conformational modifiers. A sequence was discarded if any of the remaining 18 amino acids was represented in more than 25% of the sequence (i.e. more than twice in an 8-AA-long peptide, more than 3 times in a 12-mer). The sequence was discarded if it contained more than 45% of charged (E, D, K, R, H) or hydrophobic (W, I, L, F, M, V, Y) amino acids. The sequence was discarded if it contained too many (typically more than 75%) amino acids prone to gel formation (S, T, E, D, K, R, H, N, Q, Y). If the total charge of the generated peptide was more than +1 or less than -1, the sequence was also discarded. From the remaining sequences, those that contained two or more cysteine residues were isolated and marked for their capacity to form disulfide-bridges during peptide synthesis.

After the initial random sequence generation, 3D conformations of the resulting collection of 22.5×10^6 peptides were generated using three different initial conformations for each peptide: alpha helix, beta strand or extended. To ensure the correct identification of atom types and charges for 3D molecules, we used the internal routines of Discovery Studio to produce files in SD format, suitable for further peptide docking experiments within the CDOCKER protocol[(1)]. Each peptide was typed with the CHARMm force-field[(2)] for further analysis within Discovery Studio 2.5.5 (Accelrys Software Inc). For a schematic representation of the bioinformatics workflow, see **Fig. S1**).

Docking experiments and refinement of docking poses

The Human RANK-RANKL crystal structure[3] (PDB id: 3ME2) was used to construct models of virtual peptides in complex with the RANK ligand-binding domain. Docking experiments were performed with peptides in the putative binding region on RANK using the CDOCKER[1] module of Discovery Studio 2.5.5 (**Fig. S1**). An initial high throughput screening was performed with 2.5×10^4 peptides using a limited set of conformational exploration with a calculation time of ~3 min/peptide on a dual quad-core 2.66 Ghz Xeon 5630 workstation. The most promising candidates selected after docking validation of the RANK binding energy and the quality of the pose (~100), were subjected to a refined docking analysis (with a calculation time of 24 h per peptide) for a better characterization of the most favorable RANK-peptide interactions.

Osteoblast differentiation assay

To evaluate the effect of Pep8 on osteoblast differentiation, human mesenchymal stem cells (hMSCs) from bone marrow aspirates of healthy donors were seeded in 96-well cell culture plates (3500 cells/well) and cultured for three days in DMEM-high glucose supplemented with 10% FBS (Lonza) and 100-100 µg/mL penicillin-streptomycin (Gibco). After three days, the medium was exchanged for differentiation medium containing 10^{-8} M vitamin D3 and 10^{-8} M dexamethasone (both Sigma-Aldrich) with or without different concentrations of Pep8 (5-100 µM), and cells were cultured for another 96 hours. Then, the medium was exchanged for mineralizing medium composing of DMEM/FBS-10%, 10^{-8} M vitamin D3, 10^{-8} M dexamethasone, 50 µg/mL ascorbic acid and 10 mM β-glycerophosphate (all from Sigma) with or without the treatment, and cells were cultured for an additional 2 weeks prior to Alizarin Red S staining. During this period, media and treatments of the cultured cells were replaced every 3-4 days. At 20 days, mineralized matrix nodules were stained for calcium precipitation using Alizarin Red S staining. Briefly, the medium was removed, and the cell layers were rinsed with PBS and fixed in cold 70% ethanol for 1 hour at 4°C. The cell layers were then washed several times with deionized water, and the fixed cells were incubated with 40 mM Alizarin Red S, pH 7.4 (Merck) for 10 min at room temperature, followed by extensive washing with distilled water.

The staining of calcium mineral deposits was observed both grossly and under inverted light microscope.

HEK239 cells constitutively expressing RANK

Human embryonic kidney 293 cells (ATCC number: CRL-1573) were grown in DMEM, supplemented with 10% FBS in a 5% CO_2 incubator. The cells were transduced with an expression-ready vector (Ex-O0007-Lv105, OmicsLinkTM Expression Clone, GeneCopoeiaTM, USA) containing the ORF cDNA of TNFRSF11A (accession number NM_003839.1). Briefly, cells in 6-well plates (3×10^5 cells/well) were transduced with 4 µg of the cDNA clone using Lipofectamin2000 (Invitrogen), according to the manufacturer's instructions. The cells were incubated at 37°C in a CO_2 incubator for 48 hours prior to testing for transgene expression. Then, cells were exposed to puromycin (2 µg/mL) to select for stable transfectants. Stably transfected clones were serially passaged twice per week and analyzed for RANK expression by flow cytometry (Beckman Coulter), using a primary antibody to human RANK/TNFRSF11A (R&D Systems, AF683) and an Alexa-Fluor-488-conjugated secondary antibody (R&D Systems).

FIGURES

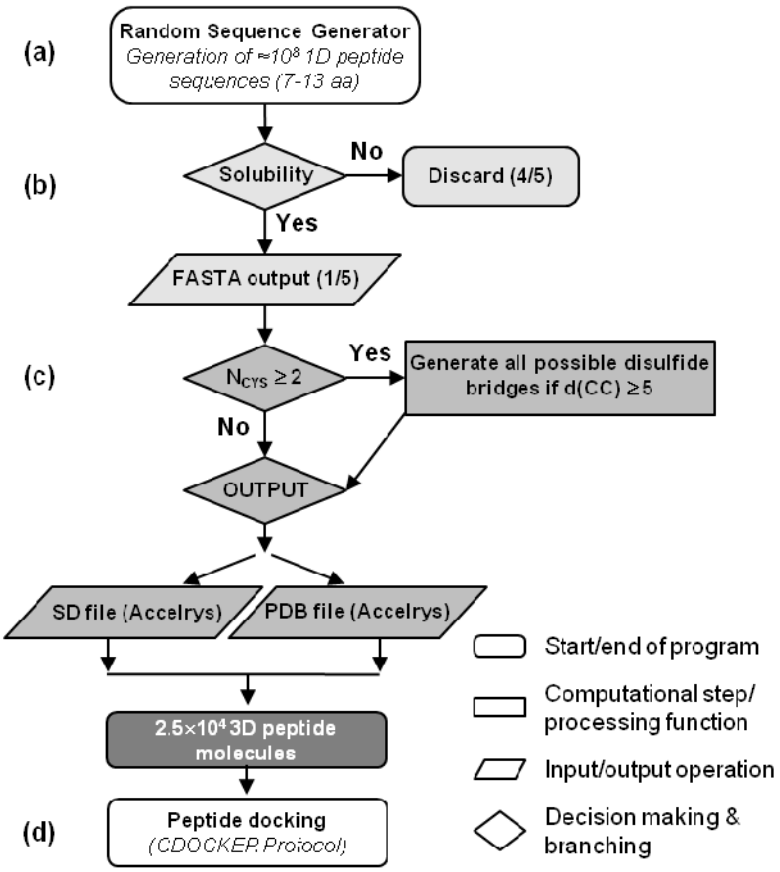

Fig. S1. Bioinformatics work-flow to generate small peptide RANK antagonists. **(a)** Generation of 1D sequences of variable length (~10^8 sequences, 7-13 AAs). **(b)** In silico filtration of sequences for aqueous solubility. **(c)** Conversion of 1D peptide sequences into 3D-coordinate molecules. **(d)** Peptide docking experiments and refined docking analysis of the most promising candidates.

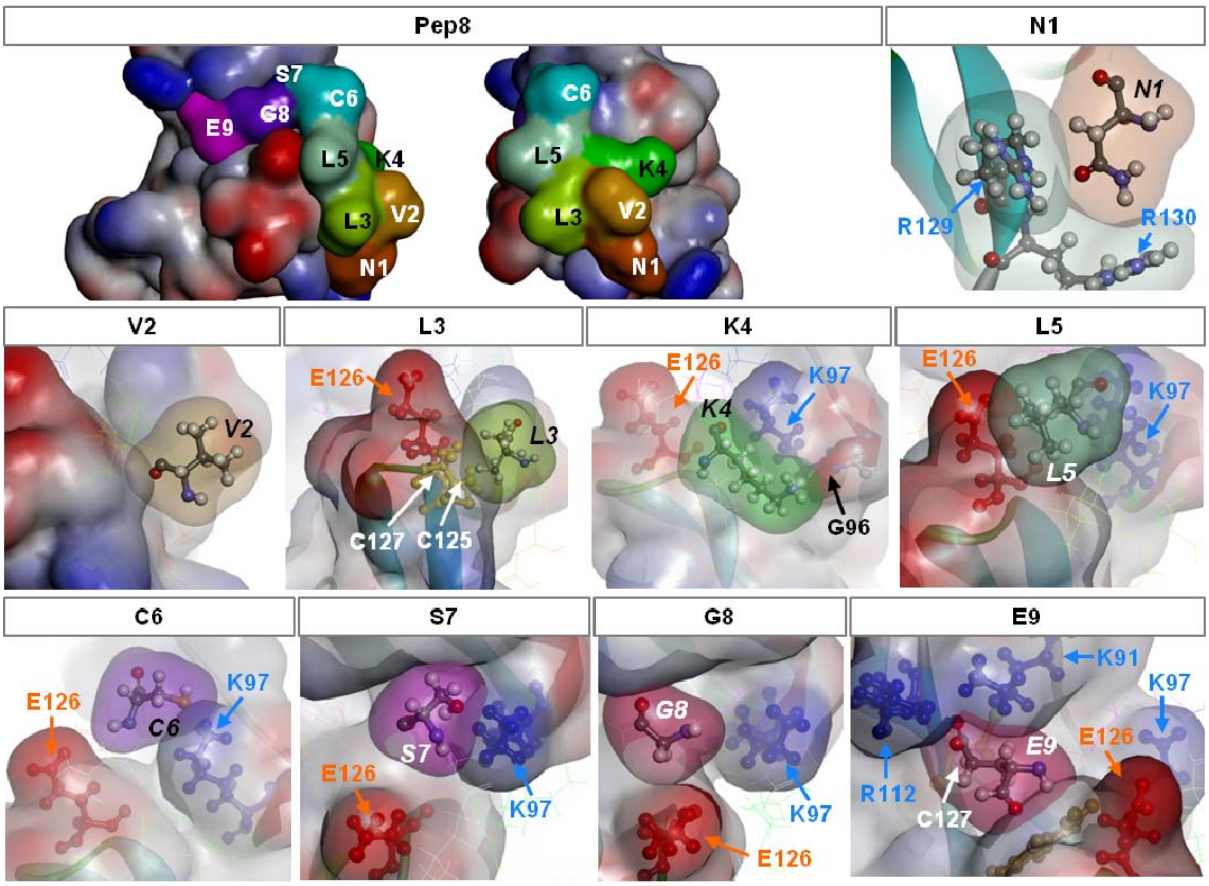

Fig. S2. Predicted molecular interactions between Pep8 and RANK. Pep8 binding to RANK; AA positions of Pep8 in the binding groove on RANK (*top row*) and individual contributions of Pep8 residues to receptor binding and activity are shown. **N1** forms a hydrogen (H) bond with RANK-R129 (which may also be formed with R130, depending on the conformation) and van der Waals interactions with R130. (*Second row*) **V2** is not in direct contact with RANK (except for the main peptide backbone chain), and is involved in RANKL repulsion. It also locks the conformation of N1, limiting contacts with R129/R130. **L3** engages in hydrophobic interactions with the C125/C127 disulfide bridge involved in the conformational lock of E126. **K4** is also involved in hydrophobic interactions (with the side chain of K97) and forms a weak H-bond with the backbone of G96. **L5** shields E126 from RANKL, thereby participating in a repulsion activity (competition) for RANKL. No direct interaction with E126, since hydrophobic-to-charges contacts are not favourable. (*Third row*) **C6** is involved in the formation of a direct S-H bond between the cysteine-SH and the hydrogen atoms of Nε of K97. This interaction contributes to the selectivity and specificity of Pep8 for RANK. **S7**, similar to C6, is involved in a direct hydrogen (OH---H) bond with K97. **G8** serves as a linker between the "competitive" part of the peptide and the part conferring RANK-affinity, since there is no room for a side-chain at this position. **E9** is involved in the formation of three H-bonds in the side chain with K91 and R112, and the main chain with C113.

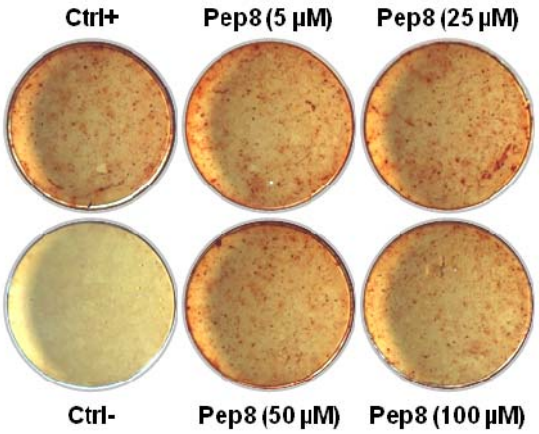

Fig. S3. Effect of Pep8 on osteoblast differentiation. Human mesenchymal stem cells (hMSCs) from bone marrow aspirates of healthy donors were grown in osteoblast differentiation medium in the presence of absence of Pep8 (5-100 µM). At the end of the experiment, cells were stained for calcium precipitation with Alizarin Red S. Photomicrographs show no significant change in Alizarin Red staining in cells treated with Pep8 compared to vehicle treated cells.

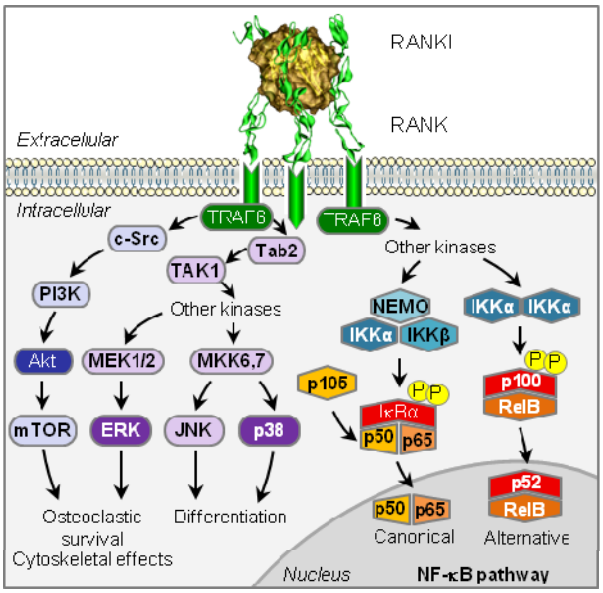

Fig. S4. RANK signaling pathways. Initial binding of TRAF6 to the cytoplasmic domain of RANK results in the activation of distinct signaling cascades regulating osteoclast differentiation and activation. Downstream targets of TRAF6 include MAP kinases, such as JNK, p38 and ERK, components of the PI3K/Akt pathway, as well as transcription factors such as NF-κB p105/p50, p65 (RelA), p100/p52 and RelB.

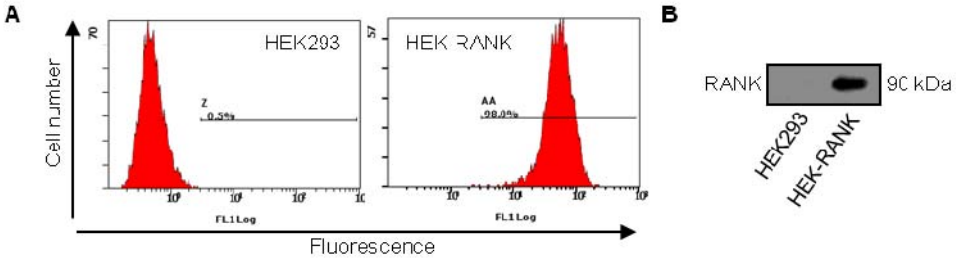

Fig. S5. HEK293 cells overexpressing RANK (HEK-RANK). **(A)** HEK293 cells were stably transduced to express RANK as described in *Materials and Methods*. A stably transfected clone was analyzed for RANK expression by flow cytometry, using primary human *RANK*/TNFRSF11A and secondary Alexa-Fluor-488-conjugated antibodies. **(B)** RANK expression was confirmed at the protein level by immunoblotting. Total cell lysates of HEK-RANK cells compared to untransfected control cells (40 µg of protein) were immunoblotted with a *RANK*/TNFRSF11A antibody.

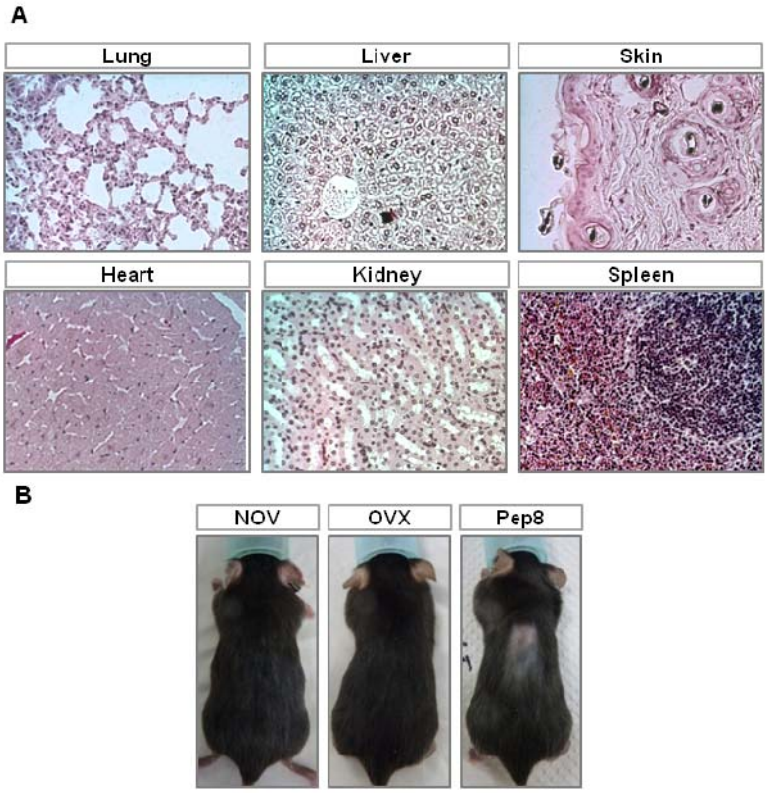

Fig. S6. Organ toxicity and side effects in OVX mice treated with Pep8. **(A)** After treatment with Pep8 or vehicle for 5 weeks, internal organs were harvested, fixed and paraffin-embedded. Sections (4 µm) were cut and stained with hematoxylin/eosin[4;5], and general morphology of organs was evaluated on each section using a DMRXA microscope (Leica) to assess for potential effects of Pep8 treatment on the organ morphology and cellular damage. Representative images of Pep8-treated mice are shown. Histopathological examination of major organs revealed no alterations that could be associated with administration of the peptide. **(B)** Transient hair loss close to the injection site was observed in 7/8 mice in the treatment group. Representative photos of mice from each group (NOV healthy controls, OVX and Pep8-treated) from week 4 of the treatment period are shown.

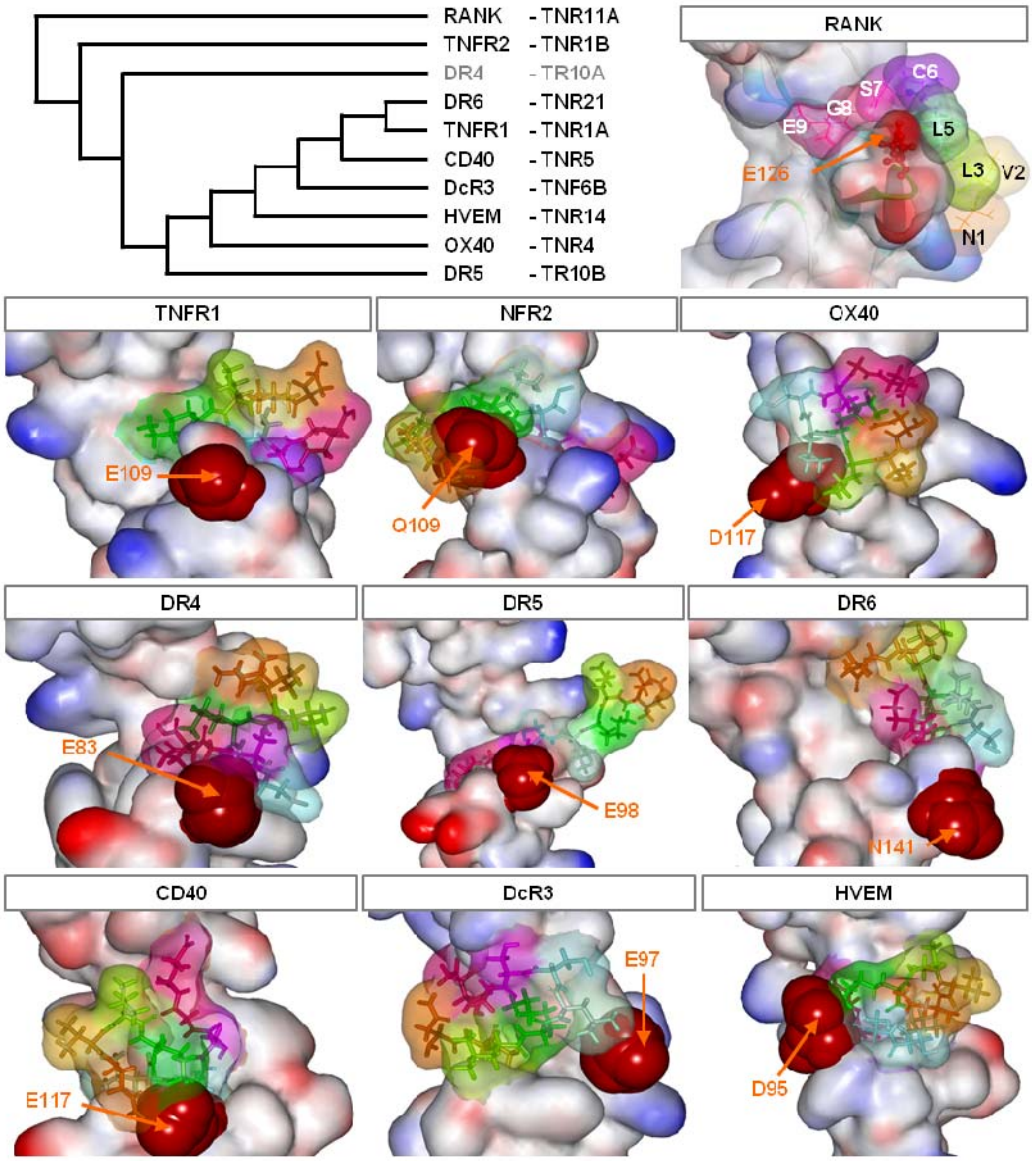

Fig. S7. Docking results of Pep8 on various TNF-R members. A phylogenetic tree produced with Seaview[6] shows the relative proximity of RANK with other members of the TNFR family (top left). Images of TNF-R members from experimental structures[3;7–14] and the DR4 model structure (derived from the DR5 crystallographic structure[15;16] in complex with Pep8 are shown. Unlike for RANK, no extended binding cavity could be defined on other TNF-R members. The AA equivalent to RANK-E126 (CPK representation in red) was identified manually from the crystal structure of the corresponding TNF receptor/ligand complex. DR6 has no bound ligand and displays an open conformation, with no potential binding groove for the peptide. Docking experiments suggested that no Pep8 conformation is able to wrap properly around the targeted AA to block ligand binding. Only some Pep8 residues are able to nonspecifically bind to a receptor. The core motif LKLCS, responsible for RANK-specificity, is often exposed to the solvent or involved in internal peptide interactions rather than interactions with the protein.

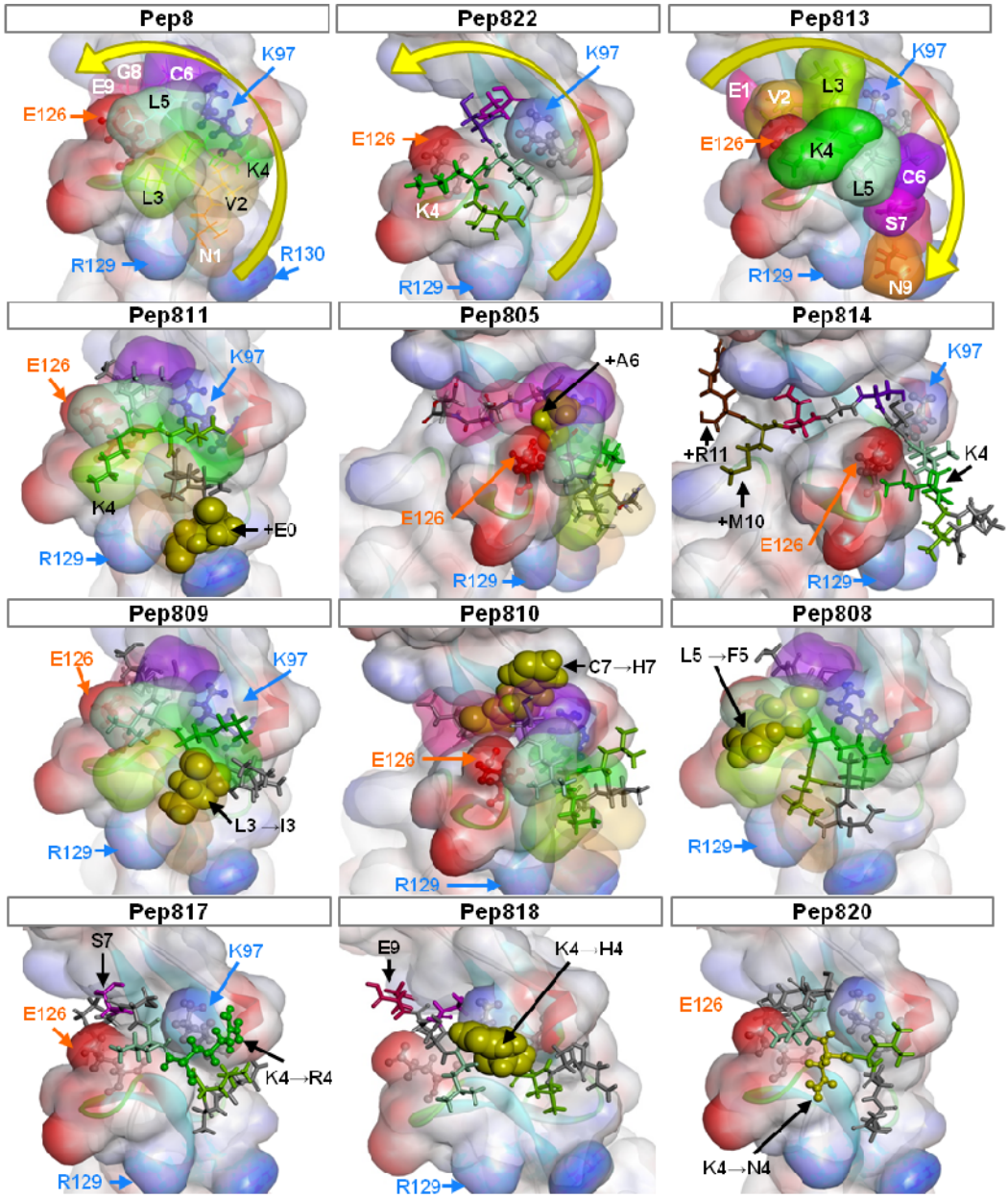

Fig. S8. Representative docking results of Pep8 derivatives bound to RANK. RANK-AA substitutions are in yellow (CPK representation). (*Top row*) Pep8 orientation and sequence is presented for references; main AAs of RANK defining the binding crevice are indicated (arrows). Yellow arrow indicates peptide orientation on RANK. (*Second row*) Increasing peptide length at N- (Pep811) or C-terminus (Pep805, Pep814) displaces K4 from its optimal position. (*Third row*) Modifying the conformational state of L3 (Pep809) or increasing the positional lock of C7 or L5 (Pep810 and 808) results in a displacement of the peptide N-terminus. The additional decrease in C-terminal peptide entropy induced by these changes is counter-balanced by the loss of binding at the N-terminus, although the K4 orientation is kept. (*Bottom row*) Loss of interactions of the positively charged K4 with RANK can be compensated by the formation of alternative interactions.

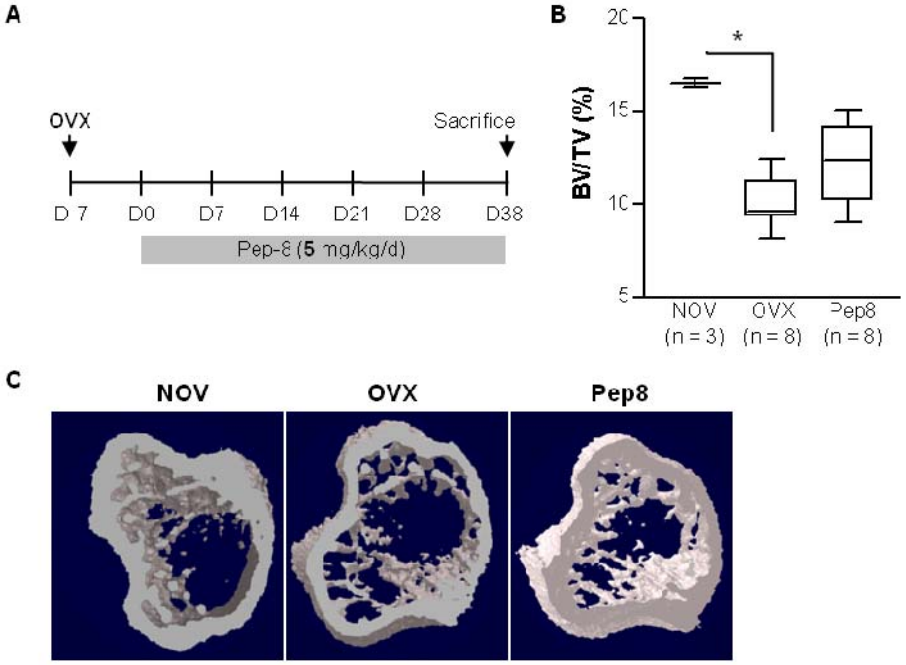

Fig. S9. Effect of Pep8 at 5 mg/kg/d on bone loss in OVX mice**. (A)** Five-week-old OVX female C57/bl6 mice received daily subcutaneous injections of 5 mg/kg Pep8 or vehicle (PBS). Non-ovariectomized control mice (NOV) were included as healthy controls and treated with the vehicle only. **(B)** After sacrifice, left hind limbs were subjected to micro-CT analysis. Analysis of architectural variables of tibiae was performed using the high-resolution X-ray micro-CT system for small animal imaging SkyScan-1076. For calculation of trabecular BV/TV, fifty slices (1 mm) at ~0.4 µm distal to the growth plate were used. Data are expressed as mean ± SEM. *$p <$ 0.01 using ANOVA and Dunnett's posttest. **(C)** Representative 3-dimensional representations of 25 slices are shown.

Table S1. Primer sequences and PCR conditions for real time PCR analysis

Name	Primer sequence	PCR conditions
CATHK	(for) 5'-GCCAGACAACAGATTTCCATC	98°C $^{30\ sec}$ × 1 cycle
	(rev) 5'-CAGAGCAAAGCTCACCACAG	(95°C $^{15\ sec}$ -60°C $^{30\ sec}$) × 40 cycles
NFATc1	(for) 5'-GGTCTTCGGGAGAGGAGAAA	98°C $^{30\ sec}$ × 1 cycle
	(rev) 5'-TGACGTTGGAGGATGCATAG	(95°C $^{15\ sec}$ -60°C $^{30\ sec}$) × 40 cycles
GAPDH	(for) 5'-TGGGTGTGAACCATGAGAAGTATG	98°C $^{30\ sec}$ × 1 cycle
	(rev) 5'-GGTGCAGGAGGCATTGCT	(95°C $^{15\ sec}$ -60°C $^{30\ sec}$) × 40 cycles
B2M	(for) 5'-TTCTGGCCTGGAGGCTATC	98°C $^{30\ sec}$ × 1 cycle
	(rev) 5'-TCAGGAAATTTGACTTTCCATTC	(95°C $^{15\ sec}$ -60°C $^{30\ sec}$) × 40 cycles
ACTB	(for) 5'-CCAACCGCGAGAAGATGA	98°C $^{30\ sec}$ × 1 cycle
	(rev) 5'-CCAGAGGCGTACAGGGATAG	(95°C $^{15\ sec}$ -60°C $^{30\ sec}$) × 40 cycles
TRAP	(for) 5'-AAGACTCACTGGGTGGCTTTG	98°C $^{30\ sec}$ × 1 cycle
	(rev) 5'-GGCAGTCATGGGAGTTCAGG	(60°C $^{30\ sec}$ -79°C $^{30\ sec}$) × 40 cycles

Features of gene specific forward (for) and reverse (rev) primers used for RT-PCR analysis. Primers were designed with Primer 0.5 software (Whitehead Institute for Biomedical Research). Reaction products were characterized by melting point determination (55-95°C with 0.5°C sec^{-1}).

Table S2. Sequences and targets of small inhibitory peptides

Peptide	Sequence	Target
OP3-4	YCEIFCYLIR	RANKL
WP9QY	YCWSQYLCY	RANKL/TNFα
Pep401[a]	ELASFNKITQLG	RANK
Pep402	ELASFNRITQLG	RANK
Pep501[a]	ELASFLKISQLG	RANK
Pep8	NVLKLCSGE	RANK
PepA11	NFECKVFAKDANM	RANK
PepA12	VDHLFKTAVENNG	RANK
PepA13	MVLHNKSSDDYNI	RANK
PepA17	WLETRLTNHMELQ	RANK
PepA18	AKFHGELMADQWQ	RANK
PepA19	NEMDLPKKSCLMN	RANK
PepA20	WAARLGDPT	RANK

[a]Hydrophobic peptides were prepared in PBS/DMSO-1%. Cysteine disulfide bonds for cyclic peptides are marked "C".

Table S3. Pep8 derivatives sharing ≥80% sequence identity*

Name	Sequence	Rationale for modification and docking prediction	*in vitro* activiy
Pep8	NV**LKLCS**GE		+++
Pep801	ELANV**LKLCS**GE	N-terminal addition of ELA to increase RANK binding	+++
Pep802	NV**LKLCS**GEAY	C-terminal addition of AY to increase affinity for RANK in the non-competitive region	+++
Pep803	ELANV**LKLCS**GEAY	Combination of 801/802	++
Pep804	NV**LKLCS**GEAYR	C-terminal addition of R to further increase interactions with RANK	+++
Pep805	NV**LKLACS**GE	The strong interaction of C6/S7 with K97 may limit peptide flexibility. Insertion of A to add room and help surround K97 better.	+++
Pep806	NV**LKLCS**E	Deletion of G between S7 and E9 to investigate whether the space between S7/E9 is needed. Molecular modeling predicts multiple possible contacts of E9 to other AAs. **In silico binding affinity is unclear.**	+
Pep807	NV**LKLSC**GE	Permutation of C6/S7 to confirm importance of hydrogen bond order (and position S7). **Lower binding affinity predicted.**	+
Pep808	NV**LKFCS**GE	Since L5 is involved in blocking RANKL-contact with E126, increasing the size of the AA in position 5 should increase repulsion. Good binding predicted *in silico*, but the bigger size of F may disturb the rest of the peptide interactions with RANK.	+++
Pep809	NV**IKLCS**GE	L3 is also involved in blocking RANK/RANKL interaction. Exchange of L for I changes the position of the CH_3 groups. This change is predicted to displace N1 from its location between R129 and R130. Should decrease peptide activity.	++
Pep810	NV**LKLCH**GE	Increasing the charged contacts using a bigger AA (H) with a clear positive charge should replace the S-H hydrogen bond formed by S and provide better binding; however, the size of H may counterbalance the gain in charge.	+++
Pep811	ENV**LKLCS**GE	Increasing the number of polar and charged groups at the N-terminus should facilitate contact to R129/130 (and possibly insert E9 between them). Good binding predicted *in silico*. K4 probably adopts the alternative binding conformation (pointing towards E126).	+++

Table S3. *Continued*

Name	Sequence	Rationale for modification and docking prediction	*in vitro* activiy
Pep812	NA**LKLCS**GE	V2 seems too big to allow N1 to correctly interact with R129/130. For more flexibility on the N-terminus, a shorter hydrophobic AA (A) was introduced. Good *in silico* binding predicted.	+++
Pep813	EV**LKLCS**GN	Exchange of N- and C-terminal AAs should not significantly alter peptide binding affinity (E and N both potentially have a close hydrogen bond network)	+++
Pep814	NA**LKLCS**GEMR	Increasing peptide length at the C-terminus should achieve stronger binding to RANK. This should increase the affinity of the peptide for RANK, but may diminish the competition activity for RANKL. **In silico prediction is unclear**: the addition of MR leads to a displacement of the peptide in the binding groove, increasing RANK binding, while at the same time decreasing the ability to block access of RANKL to RANK.	+
Pep815	NA**LKLACS**GE	As in 805, the modification is intended to relax peptide interactions around K97 for better access of N1 to R130/129 and should allow more flexibility of K4 for better contacts.	++
Pep816	NA**LKLFCS**GE	Similar to 816, the modification is intended to increase the hydrophobic contact with a bigger hydrophobic AA (F)	++
Pep817	NA**LRLCS**GE	Changing K to R may alter some interactions, but the loss of interactions of the positively charged K with RANK maybe compensated by the formation of alternative interactions. Good binding predicted *in silico*.	++
Pep818	NA**LHLCS**GE	as 819, change of K4 to H	+++
Pep819	NA**LFLCS**GE	as 819, change of K4 to F	+++
Pep820	NA**LNLCS**GE	as 819, change of K4 to N	++
Pep821	G**C**L**N**K**S**EV**L**	Scrambled control, **no or nearly no binding predicted.**	-
Pep822	**LKLCS**	The core sequence alone should not be active since, even if it binds correctly to RANK, it should not be big enough to block RANKL. **No activity predicted.**	-
Pep823	YCNV**LKLCS**GECY	Addition of two C for cyclization to increase bioavailability while maintaining peptide activity. **In silico docking predicts loss of binding affinity.**	not soluble
Pep824	NA**LKHCS**GE	Change of L5 to H to further block the access to E126 by using an AA with a higher charge.	+++

*European patent number EP11306766.4 – 210

REFERENCES

1. Wu G, Robertson DH, III CLB, Vieth M. Detailed analysis of grid-based molecular docking: A case study of CDOCKER - A CHARMm-based MD docking algorithm. J Comp Chem. 2003;24(13):1549–62.
2. Brooks BR, Bruccoleri RE, Olafson BD, States DJ, Swaminathan S, Karplus M. CHARMM: A program for macromolecular energy, minimization, and dynamics calculations. J Comp Chem. 1983;4(2):187–217.
3. Liu C, Walter TS, Huang P, Zhang S, Zhu X, Wu Y, Wedderburn LR, Tang P, Owens RJ, Stuart DI, Ren J, Gao B. Structural and functional insights of RANKL-RANK interaction and signaling. J Immunol. 2010;184(12):6910–19.
4. Baud'Huin M, Renault R, Charrier C, Riet A, Moreau A, Brion R, Gouin F, Duplomb L, Heymann D. Interleukin-34 is expressed by giant cell tumours of bone and plays a key role in RANKL-induced osteoclastogenesis. J Pathol. 2010;221(1):77–86.
5. Lamoureux F, Picarda G, Garrigue-Antar L, Baud'huin M, Trichet V, Vidal A, Miot-Noirault E, Pitard B, Heymann D, Rédini F. Glycosaminoglycans as potential regulators of osteoprotegerin therapeutic activity in osteosarcoma. Cancer Res. 2009;69(2):526–36.
6. Galtier N, Gouy M, Gautier C. SEAVIEW and PHYLO_WIN: two graphic tools for sequence alignment and molecular phylogeny. Comput Appl Biosci. 1996;12(6):543–8.
7. Banner DW, D'Arcy A, Janes W, Gentz R, Schoenfeld HJ, Broger C, Loetscher H, Lesslauer W. Crystal structure of the soluble human 55 kd TNF receptor-human TNF beta complex: implications for TNF receptor activation. Cell. 1993;73(3):431–45.
8. Mukai Y, Nakamura T, Yoshikawa M, Yoshioka Y, Tsunoda S, Nakagawa S, Yamagata Y, Tsutsumi Y. Solution of the structure of the TNF-TNFR2 complex. Sci Signal 2010;3:ra83-.
9. Compaan DM, Gonzalez LC, Tom I, Loyet KM, Eaton D, Hymowitz SG. Attenuating lymphocyte activity: the crystal structure of the BTLA–HVEM complex. J Biol Chem. 2005;280(47):39553–61.
10. Zhan C, Patskovsky Y, Yan Q, Li Z, Ramagopal U, Cheng H, Brenowitz M, Hui X, Nathenson SG, Almo SC. Decoy strategies: the structure of TL1A:DcR3 complex. Structure. 2011;19(2):162–71.
11. Cha SS, Sung BJ, Kim YA, Song YL, Kim HJ, Kim S, Lee MS, Oh BH. Crystal structure of TRAIL-DR5 complex identifies a critical role of the unique frame insertion in conferring recognition specificity. J Biol Chem. 2000;275(40):31171–7.
12. Kuester M, Kemmerzehl S, Dahms SO, Roeser D, Than ME. The crystal structure of death receptor 6 (DR6): A potential receptor of the amyloid precursor protein (APP). J Mol Biol. 2011;409(2):189–201.
13. An HJ, Kim YJ, Song DH, Park BS, Kim HM, Lee JD, Paik SG, Lee JO, Lee H. Crystallographic and mutational analysis of the CD40-CD154 complex and its implications for receptor activation. J Biol Chem. 2011;286(13):11226–35.

14. Compaan DM, Hymowitz SG. The crystal structure of the costimulatory OX40-OX40L complex. Structure. 2006;14(8):1321–30.
15. Mongkolsapaya J, Grimes JM, Chen N, Xu XN, Stuart DI, Jones EY, Screaton GR. Structure of the TRAIL-DR5 complex reveals mechanisms conferring specificity in apoptotic initiation. Nat Struct Biol. 1999;6(11):1048–53.
16. Picarda G, Surget S, Guiho R, Téletchéa S, Berreur M, Tirode F, Pellat-Deceunynck C, Heymann D, Trichet V, Rédini F. A functional, new short isoform of death receptor 4 in Ewing's sarcoma cell lines may be involved in TRAIL sensitivity/resistance mechanisms. Mol Cancer Res. 2012;10(3):336–46.